Pure appl. geophys. 158 (2001) 1377–1399
0033–4553/01/081377–23 $ 1.50 + 0.20/0

Pure and Applied Geophysics

Global Models of Surface Wave Group Velocity

ERIK W. F. LARSON[1] and GÖRAN EKSTRÖM[1]

Abstract — Measurements of group velocity are derived from phase-velocity dispersion curves and modeled with global laterally-varying isotropic structure. Maps for both Love and Rayleigh waves are created in the period range 35 s to 175 s. The data set of group-velocity measurements includes over 50,000 minor-arc observations and 5,000 major-arc observations. The errors in the measurements are estimated by an empirical method of comparing pairwise-similar paths, resulting in uncertainties which are 20% to 40% of the size of the typical measurement. The models are determined by least-squares inversion for spherical harmonic maps expanded up to degree 40. This parameterization allows for resolution of structures as small as 500 km. The models explain 70–98% of the variance relative to the Preliminary Reference Earth Model (PREM). For the area of Eurasia, the group-velocity maps from this study are compared with those of RITZWOLLER and LEVSHIN (1998). The results of the two studies are in very good agreement, particularly in terms of spatial correlation. The models also agree in amplitude at wavelengths longer than 30 degrees. For shorter wavelengths, the agreement is good only for models at short periods. The global maps are useful for prediction of group arrival times, for revealing tectonic structures, for determination of seismic event locations and source parameters, and as a basis for regional group-velocity studies.

Key words: Surface waves, Love wave, Rayleigh waves, group velocity, tomography.

1. Introduction

In recent years there have been parallel efforts to use surface waves to determine upper mantle seismic velocities. Regional studies usually model surface-wave group velocity, and global studies typically model phase velocity. Some groups have also modeled phase velocities on a regional scale (e.g., CURTIS *et al.*, 1998), however most regional studies model group velocity, for which RITZWOLLER and LEVSHIN (1998) provide an excellent recent history. There have been few studies of global group velocities, the most recent being from a decade ago – a study which had much lower resolution than is attainable today (ROSA, 1987). Several groups have recently published high-resolution global phase-velocity models (TRAMPERT and WOODHOUSE, 1996; ZHANG and LAY, 1996; LASKE and MASTERS, 1996; EKSTRÖM *et al.*, 1997; VAN HEIJST and WOODHOUSE, 1999).

[1] Department of Earth and Planetary Sciences, Harvard University, Cambridge, Massachusetts, USA. E-mail: eriklarson@post.harvard.edu

The difference between regional and global modeling has arisen partly because of the different methods of measuring phase and group arrival times. The group arrival time is easier to determine as a function of frequency, as the effects of the source generally are ignored. Variations on the frequency-time analysis method are routinely used for this purpose (DZIEWONSKI *et al.*, 1969; LEVSHIN *et al.*, 1989, 1992). There are several methods for measuring phase velocity which generally require synthetic seismograms to be generated for each path. Two "automatic" methods have recently been developed to measure many paths for global tomographic studies (TRAMPERT and WOODHOUSE, 1995; EKSTRÖM *et al.*, 1997). Also, if the phase dispersion (phase velocity as a function of frequency) has been measured for a given path, it is possible to derive the group dispersion as we show in section two.

An important difference between regional and global studies is the path coverage. In most studies all sources and stations lie within the region being modeled. For regional studies this leads to fewer data constraints near the edges of the region, and, in particular, fewer crossing paths. This can lead to large errors in the models near the edges and it is usually difficult to determine how much of the model is affected by this problem. Global models are not affected by this since all stations and earthquakes are within the region of study. Another disadvantage of the path coverage of regional studies is that all path lengths are relatively short. This can make it more difficult to measure the dispersion of long-period waves and to determine the large-scale structure.

An additional difference between measuring phase and group dispersion is the sensitivity to the source parameters. The "source phase" (due to earthquake focal geometry) must be accounted for in the measurement of phase velocities (KNOPOFF and SCHWAB, 1968). Therefore, studies measuring phase-velocity dispersion are limited to earthquakes for which source mechanisms have been determined. The Harvard centroid-moment tensor catalog (DZIEWONSKI *et al.*, 1981) provides source mechanisms, although only for large earthquakes. Since direct group-velocity measurements are insensitive to the source phase, smaller earthquakes with undetermined focal mechanisms are often used in regional group-velocity studies. A group-velocity measurement is somewhat sensitive to the depth of the earthquake, but this effect is usually ignored (LEVSHIN *et al.*, 1999). Our method for measuring group-velocity accounts for both source depth and mechanism.

Both phase-velocity and group-velocity measurements are affected by errors in source parameters (MUYZERT and SNIEDER, 1996; LEVSHIN *et al.*, 1999). These errors may be significant for an individual measurement, particularly for Rayleigh waves. However, as LEVSHIN *et al.* (1999) point out, in the resulting maps the errors typically appear only near the edges where there is poor path coverage. Therefore, global studies with very good path coverage are less affected by such errors than regional studies.

In this work we bridge the gap between the global phase-velocity studies and regional group-velocity studies by determining new high-resolution global group-

velocity models. We determine maps of surface-wave group velocities at periods ranging from 35 s to 175 s. The parameterization for the maps allows structures as small as 500 km to be modeled. These maps are directly useful in several ways: to provide group arrival-time predictions for teleseismic studies, to investigate tectonic questions with crust and upper mantle signatures, and as starting models for high-resolution regional studies. In addition, these models enable us to study carefully whether regional and global studies agree. The agreement of regional and global models has been questioned in the literature (PASSIER and SNIEDER, 1995; CHEVROT *et al.*, 1998). The resolution in this study is sufficiently high to directly compare our global maps with a continental-scale study of Eurasian group velocities (RITZWOLLER and LEVSHIN, 1998). We compare the maps both in the spatial and spectral domains. We choose the RITZWOLLER and LEVSHIN (1998) study because it is based on more data and covers a larger region than any other work, allowing the maximum area for comparison.

We make several standard assumptions in the determination of the group-velocity maps. First, we ignore the deviation of the raypaths from the great circle. For smooth models this effect has been shown to be small when the data are phase- or group-dispersion curves (WANG and DAHLEN, 1995; WANG *et al.*, 1998). The assumption of a "smooth model" is more questionable for the maps in this study with the largest amplitude anomalies (the shortest period models). Second, we do not allow for azimuthal anisotropy in our model parameterization. In most areas of the world anisotropy has been shown to be of small magnitude compared to isotropic structure, particularly at long wavelengths (NISHIMURA and FORSYTH, 1988; MONTAGNER and TANIMOTO, 1990; TRAMPERT and WOODHOUSE, 1996). For the scale and resolution of this study, the effects of anisotropy will not bias the isotropic results (LARSON *et al.*, 1998), except possibly in the eastern Pacific, where the anisotropy may be large. Third, we do not account for mislocation of earthquakes or errors in station time. These effects have been shown to be negligible in other works (RITZWOLLER and LEVSHIN, 1998; EKSTRÖM *et al.*, 1997).

2. Method and Data

The group velocity of a wave, U, is defined by the angular frequency, ω, and the wavenumber, k, as

$$U = \frac{d\omega}{dk} = c + k\frac{dc}{dk} \quad , \tag{1}$$

where $c = \omega/k$ is the phase velocity. We can substitute $k = \omega/c$ and

$$\frac{dc}{dk} = \frac{dc}{d\omega}\frac{d\omega}{dk} = \frac{dc}{d\omega}U \quad . \tag{2}$$

Then, at a particular frequency, we can express the group velocity by

$$U = \frac{c}{(\omega/c)(dc/d\omega) - 1} \quad . \tag{3}$$

Therefore, if we know the phase-velocity dispersion, $c(\omega)$, across some frequency range, we can easily calculate the group velocity $U(\omega)$ across that range.

For our purposes we wish to know the perturbation of group velocity away from some reference model, $\delta U = U - U_0$. For a surface wave recorded on a seismogram, the measurable datum is the average perturbation of the group velocity along the path from the earthquake to the station, $\overline{\delta U}$ (where the bar indicates an average). In terms of the reference phase velocity, c_0, and path-average perturbed phase velocity, $\overline{\delta c}$,

$$\overline{\delta U} = \frac{c_0 + \overline{\delta c}}{\omega/(c_0 + \overline{\delta c})((dc_0/d\omega) + (d\overline{\delta c}/d\omega)) - 1} - U_0 \quad . \tag{4}$$

If the phase-velocity dispersion of a surface wave has been measured, the average group velocity for the path from the earthquake to the station can be easily determined. For our analysis we use $\overline{\delta U}/U_0$ as the datum, with the reference velocities c_0 and U_0 from PREM (DZIEWONSKI and ANDERSON, 1981).

We measure phase-velocity dispersion using the frequency-band expansion method (EKSTRÖM *et al.*, 1997), and then calculate the frequency-dependent group-velocity perturbation. The principle of the method is to estimate the optimal phase-matched filter to fit the data. For a given path, this phase-matched filter provides the apparent average phase-velocity perturbation as a function of frequency. A key part of the method is that it expands the range of frequencies to fit, beginning with the long periods and gradually widening the range to include higher frequencies. This method has the advantage of being entirely automatic with no user interaction, allowing for the measurement of a great many paths. In addition, the method provides an estimate of the quality of each measurement (A, B, or C), which is based on the fit to the data. We sample the phase-dispersion curves, which are represented by six B-splines, at a number of frequencies and use the method above (Eq. 4) to extract the group-velocity perturbation. The range of periods for minor-arc paths is 35 s to 175 s and for major-arc paths 70 s to 175 s. In order to directly compare our maps with the maps of RITZWOLLER and LEVSHIN (1998) we sample the group-velocity dispersion curves for both Love and Rayleigh waves at 35 s, 40 s, 50 s, 60 s, 70 s, 80 s, 90 s, 100 s, 125 s, 150 s, and 175 s period.

Our data set is derived by applying the above method to digital seismograms from the Global Seismographic Network (GSN) of Incorporated Research Institutions for Seismology (IRIS), the Chinese Digital Seismograph Network (CDSN), the Global Telemetered Seismograph Network (GTSN), and the MEDNET and GEOSCOPE networks from the period 1989–1997. Earthquake source parameters are taken from the Harvard centroid-moment tensor catalog (DZIEWONSKI *et al.*, 1981). To avoid

problems associated with short paths and with caustics, only stations in the range 30° to 150° from the earthquake are used. For minor-arc paths, we determine phase-dispersion curves of seismograms from earthquakes with $M_W > 5.5$ and depth less than 50 km. We augment the data set of phase-velocity dispersion measurements used in EKSTRÖM *et al.* (1997) by approximately 50%, and use a total of 198,998 minor-arc paths. In addition, we measure major-arc paths for events with $M_W > 6.5$, resulting in 31,903 paths. We select the data based on a quality of fit parameter which is determined in the measurement process. Depending on the period of measurement, between 20% and 25% of the data satisfy the selection criteria and are retained in the data set.

We discard measurements which are outliers and appear to be in error. For minor-arc paths we remove measurements more than 2.5 standard deviations from the mean, which eliminates fewer than 2.2% of the data. For major-arc paths there are more outliers and the cut-off is reduced to 1.25 standard deviations, which removes 8–13% of the data. The number of measurements which pass the quality selection and this cut-off is shown in Table 1. The distribution of paths is typical for a global study: better in the Northern Hemisphere, although the major-arc paths help in the Southern Hemisphere. Figure 1 shows representative path coverages for Rayleigh waves at 80 s and Love waves at 35 s.

The measurement uncertainty is estimated using a method of comparing pairwise-similar paths. For all pairs of measurements recorded at a given station, we calculate the distance between the earthquakes. The distance between the earthquakes, s (separation), defines the "pairwise-similarity" of the pair. We also define the quality of the pair, q, to be the worse of the two quality values of the two measurements. In addition, we calculate the difference between the two group-velocity measurements,

Table 1

Number of measurements which pass quality check at each period

	Minor-arc		Major-arc	
Period (s)	Love	Rayleigh	Love	Rayleigh
35	24805	49477		
40	25264	50068		
45	25199	49886		
50	36895	64704		
60	36666	64556		
70	36648	64936	5030	7619
80	36564	64813	5122	7885
90	36636	65034	5003	8146
100	36479	64755	4956	8074
125	34983	63606	5018	7828
150	26345	56773	4790	7755
175	26393	56661	4586	7679

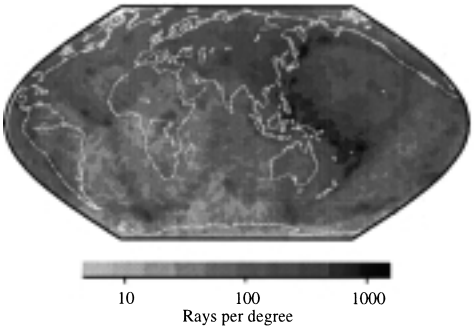

(a) Minor-arc Rayleigh wave 80 s

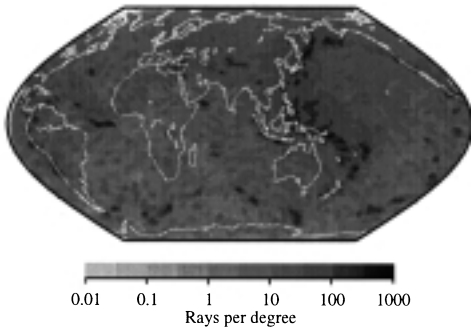

(b) Major-arc Rayleigh wave 80 s

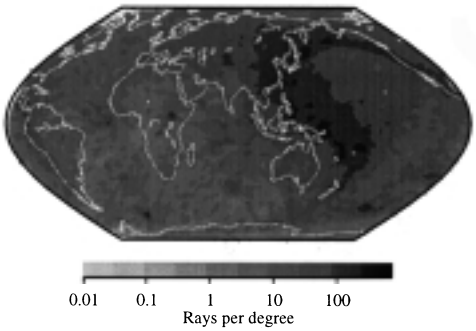

(c) Minor-arc Love wave 35 s

Figure 1
Raypath density for various models in ray degrees per $(\text{deg})^2$. The density is calculated by dividing the sum of the length of all raypaths within each cell by the area of the cell.

d. Note that d would be zero if there were no errors in the measurement or in the source parameters and the measurements were from earthquakes at the same location. We then divide the pairs into groups, for example one group is all pairs with s between 1° and 1.5° and q corresponding to 'B' quality paths. For each group we calculate one-half the root-mean-square of the differences,

$$e = \frac{1}{2}\sqrt{\frac{\sum_i^N d_i^2}{N}} \tag{5}$$

where N is the number of pairs in the group. If we have a normal distribution of errors, e is the empirical error for that group of pairs, that is if one calculates the difference between all values in a normal distribution, the root-mean-square is twice the standard deviation of the distribution.

However, the earthquakes for each pair of paths are at slightly different locations. Consequently the errors estimated by this method include the effect of the difference in group-velocity between the two paths. Since this is the signal we model, we attempt to determine and remove this effect. From Table 2 and Figure 2 we can see that the errors increase approximately linearly with separation s. The table also shows that the quality grade is quite useful – the lower quality paths have a larger error. We fit the dependence upon separation by assuming a relationship with distance for the

Table 2

Error estimates for average group-velocity perturbations $\overline{\delta U}/U_0$ (in percent) using the method of pairwise-similar paths for 80 s Rayleigh wave minor-arc data. Rows show different maximum earthquake separation distances. Columns are for different quality groups. The best fit gives a slope 0.0523%/(deg) for dependence upon distance and a "zero-distance" errors for quality A paths of 0.470%, quality B 0.715%, and quality C 0.898%. See Figure 2 for a graphical representation

Distance	Quality A	Quality B	Quality C
1.5°	0.549	0.790	0.975
1.75°	0.563	0.805	0.988
2°	0.576	0.817	1.00
2.25°	0.586	0.832	1.02
2.5°	0.597	0.846	1.03
2.75°	0.609	0.859	1.04

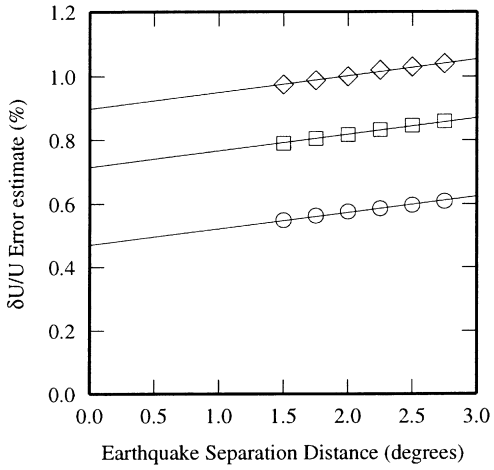

Figure 2
Example calculation of error estimates from pairwise-similar paths. Symbols are the error estimate within each category, with circles indicating best quality, squares intermediate, and diamonds are the lowest acceptable quality group. They are plotted at the maximum separation between earthquakes in their category. The straight lines are the fit to the estimate, and the y intercept is used as the error estimate for the given quality group.

errors, which is the same for all quality groups. For the error of group, e_{ij} from Equation (5), with separation in the range s_{j-1} to s_j in quality grouping i, we have

$$e_{ij} = E_i + Ss_j \ , \tag{6}$$

where E_i is the error for group i at separation zero, and S is the slope of the increase of error with earthquake separation distance. This allows us to solve for the slope and error for each quality group at each period. This is graphically represented in Figure 2. To assign uncertainties for each measurement, we assign the value E_i for the quality group of the measurement. The uncertainties range from around 0.5%, for the best quality paths, to around 1.0%. Using the uncertainties derived from this method, the initial variance of the data/uncertainty for all paths varies between 2.3 and 5.0, that is, the average uncertainty is between 20% and 40% of the measurement, depending on the frequency and wave type.

3. Inversion

To determine global group-velocity maps from individual measurements of group velocity, we follow a two-step inversion procedure. We perform the same procedure for Love and Rayleigh waves at each frequency. For 70 s period and longer, we use major-arc measurements in addition to minor-arc measurements. We weigh each datum by the inverse of its uncertainty estimate.

In the first step of the inversion we invert for a long-wavelength model. We use all measurements which satisfy our quality criteria. The basis functions are surface spherical harmonics up to degree 12, described by 169 spherical harmonic coefficients. This results in a model with minimum wavelength of 3000 km. We use a least-squares inversion, and this parameterization requires no damping or regularization. The long-wavelength model explains most (70–95%, depending on frequency) of the variance in our data.

In the second step we invert for a higher degree spherical harmonic map. The maximum degree for which we invert (and which is used for our final model) is degree 40, which allows for description of features as small as 500 km. The data are selected using the quality criteria and the predictions of the degree 12 model. All measurements that are more than 1.25 standard deviations away from the value predicted by the degree 12 model are discarded. This removes approximately 25% of the minor-arc data and 30% of the major-arc data. This is a greater number of outliers than for phase-velocity data (EKSTRÖM *et al.*, 1997), probably because the group velocity is derived from derivatives of the phase-velocity dispersion curve, which are more sensitive to errors. Of course some of these "outliers" may be correct data, but we think it is a better choice to exclude these points. For the inversion we again perform a least-squares fit to the data, but models expanded beyond degree 20 require regularization. We choose to damp the first spatial derivative of the output

model. The strength of the damping is chosen conservatively (in our opinion) to produce models which are unlikely to have spurious features, but are probably more smooth than the actual Earth.

As is typical in studies of Earth structure, the smaller scale structure only explains a fraction of the variance that remains after the large-scale structure is accounted for. In this study we explain only about 10% of the remaining variance after the degree 12 inversion, even with a degree 40 spherical harmonic map. To determine whether these fits are statistically significant, we calculate $\sqrt{\chi^2/(N-M)}$, where χ is the root-mean-square misfit, N is the number of data points, and M is the number of model parameters. This statistic becomes smaller as the degree of the model is increased, which indicates that the use of more parameters is justified (PRESS *et al.*, 1992). The remaining variance indicates that we are underestimating the errors in our data. The additional errors could result from systematic effects, such as systematically mislocated earthquakes, which are not recovered by the pairwise-similar path estimate of errors.

In Figures 3 and 4, we illustrate the fits provided by the models. Over 90% of the initial variance in the Rayleigh-wave data is explained at all periods. For Love waves, the long-period (>100 s) fits are between 80% and 90%, the intermediate periods (60–90 s) between 90% and 95%, and the short-period fits are better than 90%. The short-period Rayleigh-wave models also fit extremely well. However, this higher fit for short periods is somewhat deceptive – the initial variance is substantially higher for short periods because there are larger long-wavelength group-velocity anomalies. The final residuals are actually larger at the short periods even though the fit is better. The improvement of the high-resolution model appears very small because so much of the signal is fit by the long-wavelength model. Since our data coverage is uneven, it is impossible to further refine the long-wavelength parameters without allowing smaller scale structures in our models. The residual misfit of the predictions of the final model to the data ($\overline{\delta U}/U_0$) is about 0.6% and somewhat smaller at longer periods.

4. Maps

To illustrate our final models, we show maps at two frequencies. All of the degree 40 maps of group velocity are available electronically, as described in the Acknowledgements.

We present two maps as examples, a short-period Love-wave model (for which we have the least data), and a long-period Rayleigh-wave model (for which we have the most data). The maps are shown in Figure 5. The apparent resolution of the 90 s Rayleigh wave map is high everywhere; structures as small as 1000 km appear to be modeled globally. However, the fewer data constraints on the 40 s Love-wave map cause less small-scale structure in some poorly sampled regions, such as Antarctica.

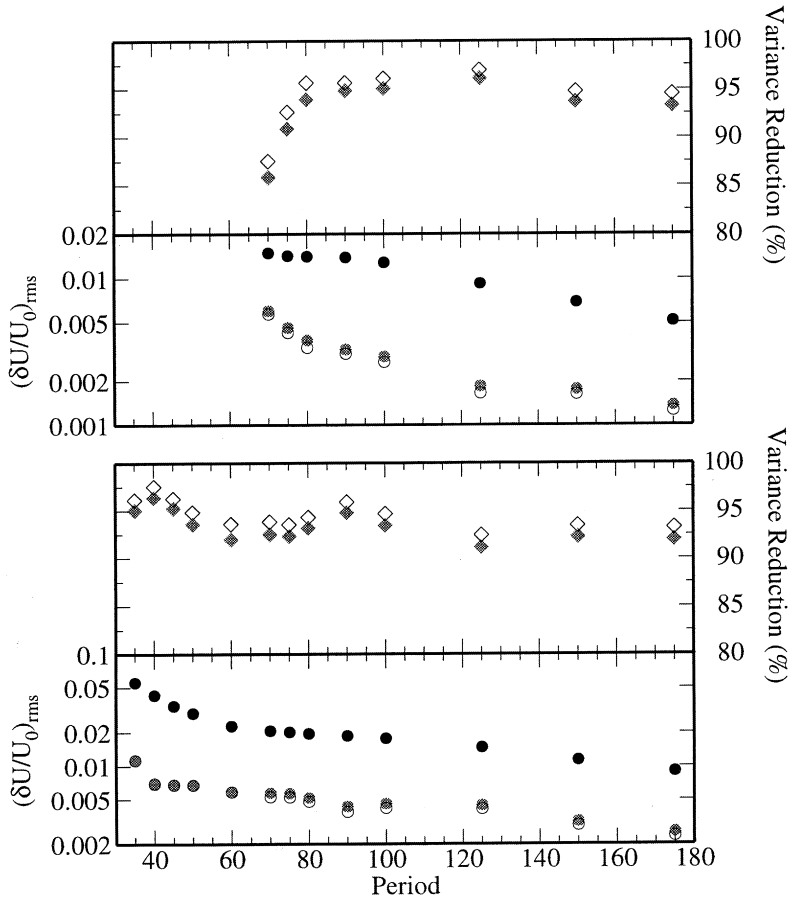

Figure 3
Fits of Rayleigh-wave models to data. Top panels are for major-arc data, bottom for minor-arc data. Solid circles are the initial root-mean-square (rms) of all measurements at each frequency, gray circles are the rms of the residual for the degree 12 models, and open circles are the rms of the residuals for the degree 40 models. The diamonds are the variance reduction to the weighted data, again, gray for the degree 12 models and open for the degree 40 models.

To understand the character of the maps, it is important to know how the group-velocity structure relates to the seismic velocities in the earth. The maps are primarily sensitive to shear-wave speeds in the crust and top few hundred kilometers of the upper mantle. The most shallow sensitivity is that of short-period Love waves, which are primarily sensitive at depths less than 30 km – crust in the continents, lithosphere in the oceans. The Rayleigh waves have a maximum sensitivity somewhat deeper (for the same frequency).

The sensitivity to differing depths leads to differences in the overall character of the models. As noted before, the short-period models have larger variations than the long-

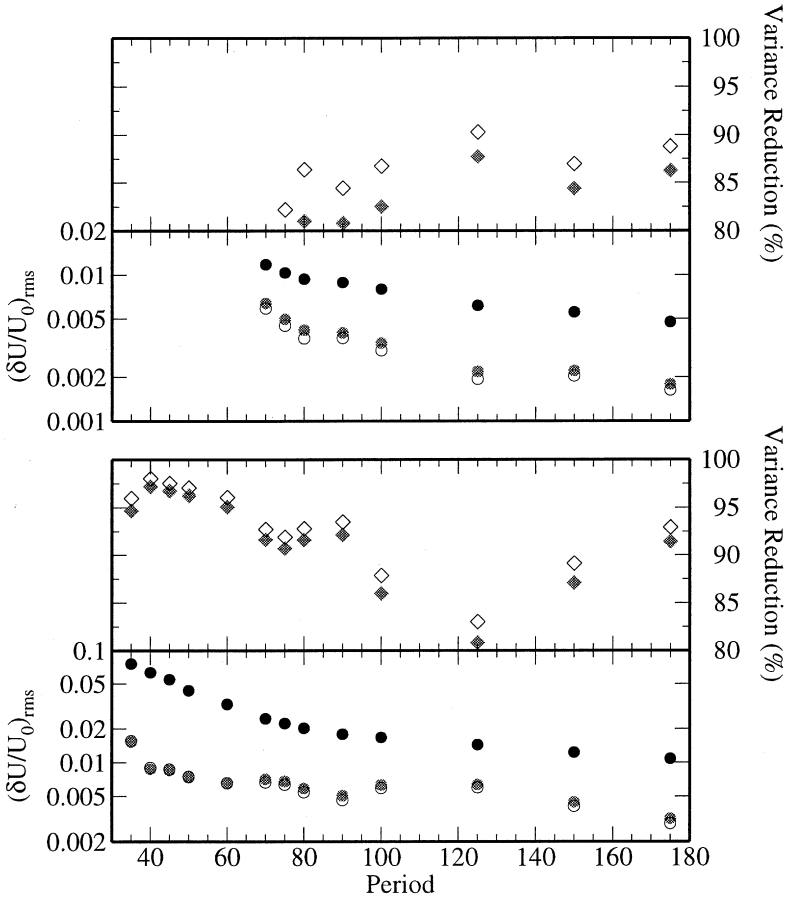

Figure 4
Fits of Love-wave models to data. See Figure 3 for explanation.

period models (as can be seen in the spectra of the models in Figs. 6 and 7). This arises because of the strong contrast at the Mohorovičić discontinuity. The spectra also show that the long-wavelength terms dominate the maps. The power in degrees greater than 12 is typically one or two orders of magnitude below the power of low-degree structures. These low-degree structures also contribute very strongly to the measurements since the variations with shorter wavelengths cancel out along the path.

The dominant features in our new maps are very similar to what has been seen previously in upper-mantle studies. The 40 s Love-wave map (Fig. 5a) matches the contrasts between oceans and continents very closely. The map images some relatively small structures such as New Zealand and the Falklands continental shelf. The thick crust of the Ontong Java plateau is also apparent. The deep crustal roots under mountain ranges appear clearly, for example under the Andes and the

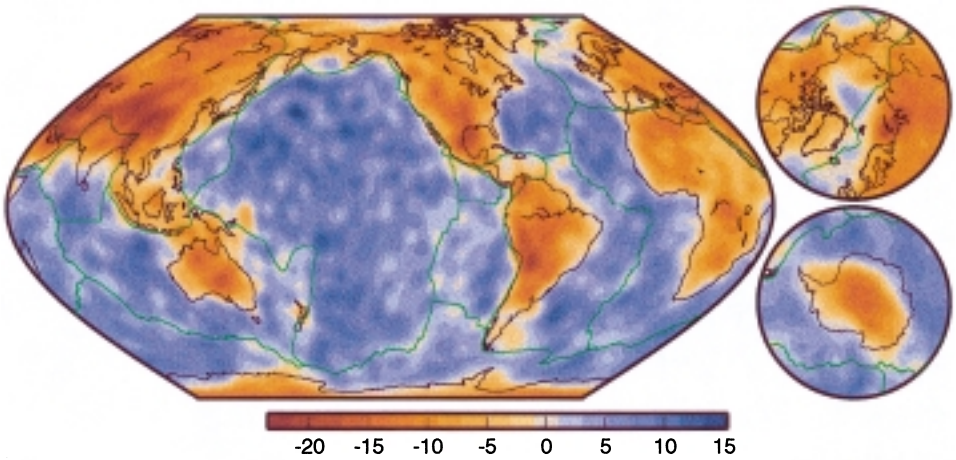

(a) Love wave 40 s

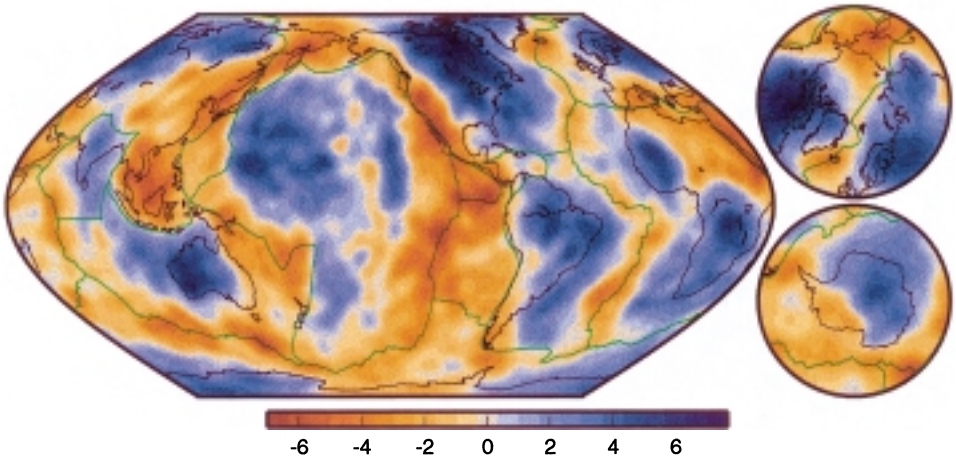

(b) Rayleigh wave 90 s

Figure 5
Group velocity in percent variations of $\delta U/U_{\mathrm{PREM}}$.

Himalayas and Tibetan Plateau. Several regions of thick sediment can be seen, such as in the Kara Sea/Barents Sea and in the Gulf of Mexico. However, elsewhere in the oceans there is little coherent structure.

The 90 s Rayleigh-wave map (Fig. 5b) presents a very different picture. This map has a maximum sensitivity to seismic velocities at roundly 100 km depth. The dominant features are high-velocity lithospheric continental roots and low-velocity

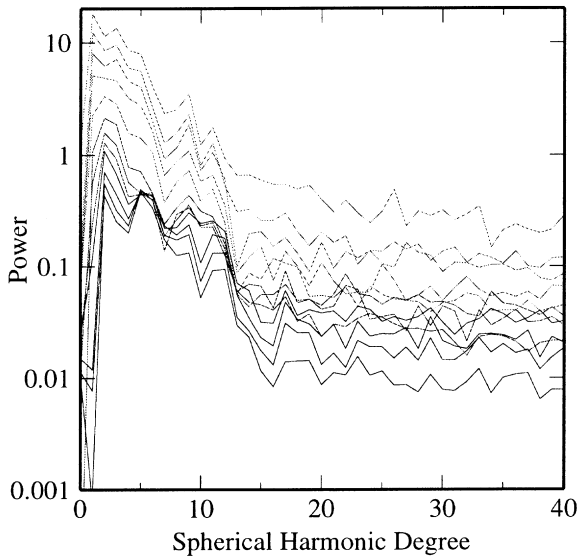

Figure 6
Spectra of Love-wave models. Maps for periods less than 60 s are lightest gray and maps 100 s and longer period are in black.

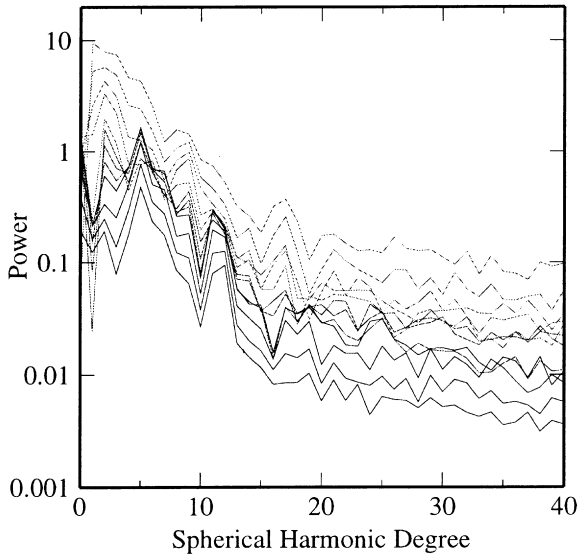

Figure 7
Spectra of Rayleigh-wave models. Maps for periods less than 60 s are lightest gray and maps 100 s and longer period are in black.

plate boundaries. One notable feature in this map is the clear division between east and west Antarctica. There are two places where the low velocities do not correspond with the plate boundaries from NUVEL-1 (DeMets *et al.*, 1990). The boundary between North America and Eurasia in Siberia appears further east in our maps, and the boundary between North and South America appears to be further south. We also note one surprising feature in the 90 s Rayleigh wave map: a north-south linear structure west-central in the Pacific. This structure appears to be a possible artefact of erroneous data, however we have confirmed that it is present in models derived from major- and minor-arc data separately. This feature may be a result of endeavoring to model azimuthally anisotropic material with an isotropic parameterization (see Larson, *et al.*, 1998, Figs. 8 and 13).

5. Comparison

To assess the agreement of global models with a regional model, we compare our maps with the high-resolution regional study of Eurasia of Ritzwoller and Levshin (1998). Figure 8a shows a visual comparison of the two studies for Love waves at 40 s, and Figure 8b is for Rayleigh waves at 100 s. It is apparent that the maps are very similar. The largest differences occur near the edge of the maps, particularly on the eastern edge of the region. This difference is due to the lack of coverage in the regional study. The global maps of this study agree with the long-established result that the lithosphere is fast under old basins (Dorman, 1969). In the central part of the maps, structures larger than about 700 km agree quite well. There are, of course, smaller scale features in the regional study, as small-scale features are not parameterized in the global modeling. Also, in the long-period map, the amplitudes of many small-scale anomalies are noticeably smaller in the global model.

In the 40 s Love-wave maps (Fig. 8a), the correlation is clear and the amplitudes agree well. As we survey the maps from north to south, we see striking agreement. Above 60°N, both models exhibit small anomalies in the east, a slow region with a maximum amplitude of about 17% in north central Russia, and various 5–10% slow anomalies in the west. Between 45°N and 60°N, there is less variation, although both models show slower regions near Belarus, at the north end of the Caspian Sea, north of the Kazakhstan-Russia western border, and northwest of Lake Baikal. The strongest anomalies are in the 30°N to 45°N range, with both models showing slow anomalies of 20–25% at the south end of the Caspian Sea and in eastern and western Tibet (but not as slow in the center). There is a sharp contrast between very slow velocities and only slightly slow anomalies west of 110°E. Between 15°N and 30°N, we again see matching strong anomalies, with both models showing regions 15–20% slow in the Persian Gulf and in Bangladesh.

In the 100 s Rayleigh-wave map (Fig. 8b), the correlation is still extremely high, but the amplitudes do not agree as well. Moving from east to west, we see a number

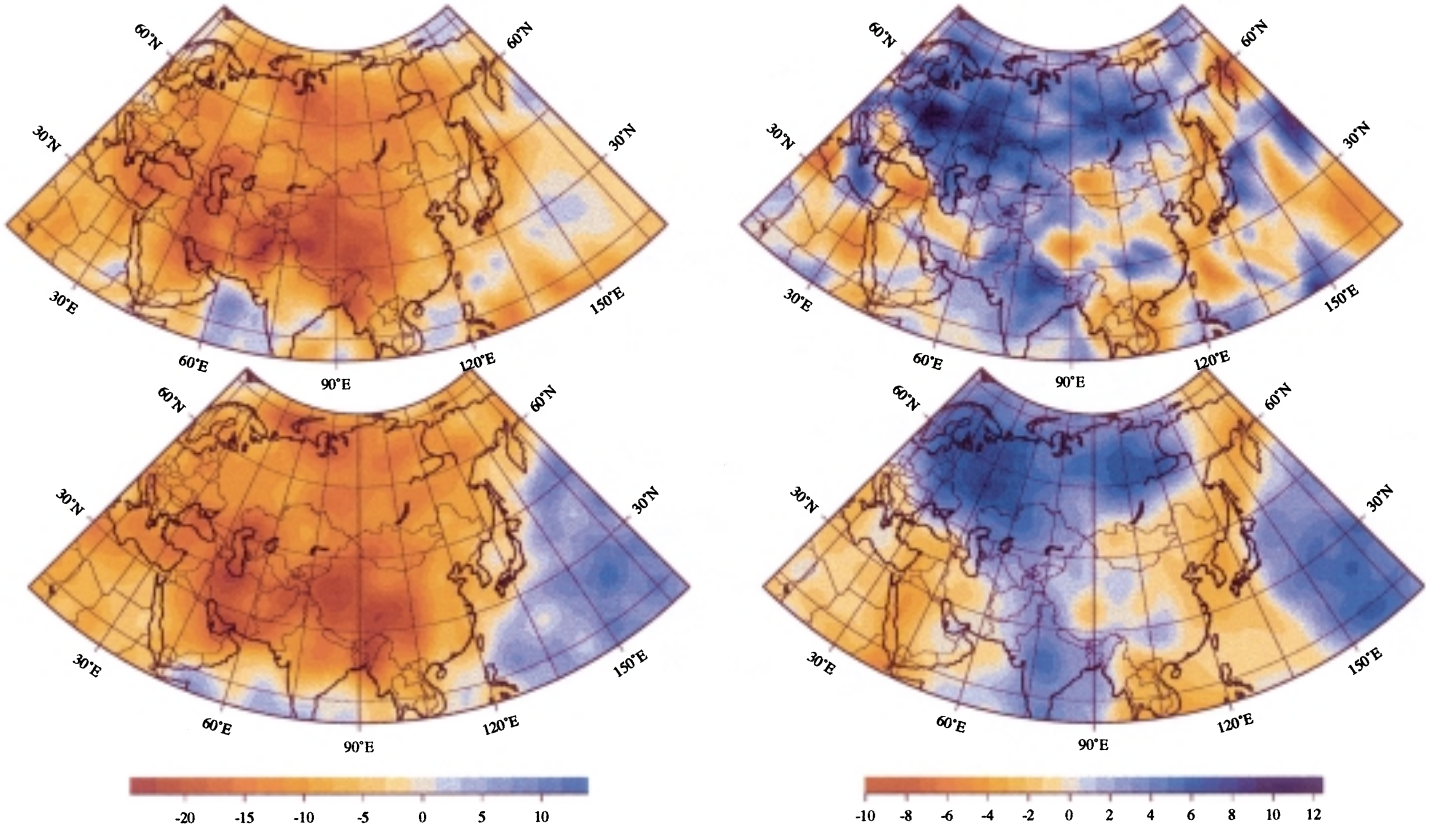

Figure 8
Comparison of group-velocity maps from RITZWOLLER and LEVSHIN (1998) study of Eurasia (top) with the global result of this study (bottom). Maps are plotted at the same scale, in percent variations of $\delta U/U_{\mathrm{PREM}}$.

of matching features. Both models recover a line of slow regions along the coast of Asia, with slower spots in Kamchatka, under Sakhalin Island, off the coast of the Korean Peninsula, and off the coast of central China. A fast region is apparent in central Siberia. A belt of slow velocity connects Tibet to the coast, and a fast region in southeast China. Southeast Asia is slow, with a maximum anomaly of 3–5%. Central Russia is slightly fast in both maps and Kazakhstan has a complex structure. Tibet is characterized as a slow anomaly, whereas India is fast (although the location of this anomaly disagrees by a few hundred kilometers). There is disagreement in European Russia – both maps show a fast region, although the regional study has considerably larger amplitudes. Turkey and Iran are slow in both studies. The studies disagree in the Arabian Sea, however the Red Sea shows a 4–5% slow anomaly in both studies. In the rest of Africa there is scant data constraining the regional model.

To further determine the agreement between the two studies, we calculate several statistical parameters. Since the errors in the RITZWOLLER and LEVSHIN (1998) maps may be large near the edges, we have chosen two smaller interior regions to compare statistically: a large region of Eurasia and a smaller region of Central Asia, as shown in Figure 9. These regions are rectangular in equal-area projections, allowing us to easily calculate a two-dimensional discrete Fourier transform. The Fourier transform of a model $f(x_i, y_j)$ over a region R of size X by Y which is discretized in N_x points in the x direction and N_y points in the y direction is (PRESS *et al.*, 1992)

$$F_{ij} = \frac{1}{\sqrt{XY}} \sum_{k=0}^{N_x-1} \sum_{l=0}^{N_y-1} e^{2\pi i x_k/\lambda_i^x} e^{2\pi i y_l/\lambda_j^y} f(x_k, y_l) \quad , \tag{7}$$

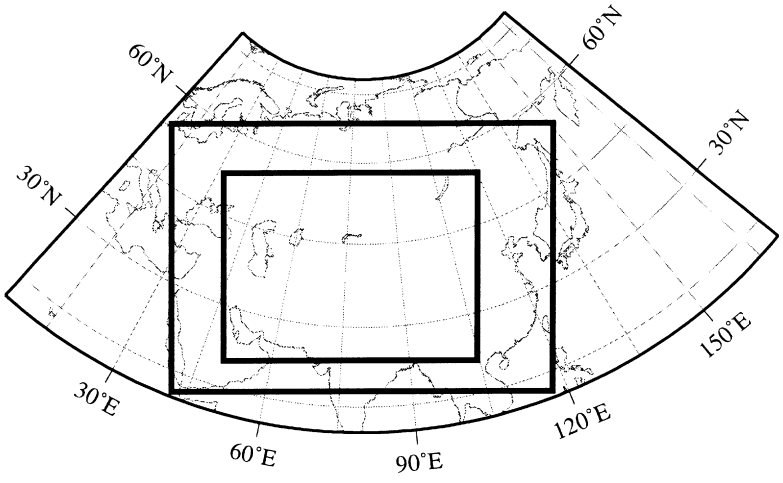

Figure 9
Boxes show regions used for statistical comparisons.

and $\lambda_m^x = X/x_m$ and $\lambda_m^y = Y/y_m$ are the wavelengths. From the Fourier transform coefficients, we calculate the amplitude spectra in the $A_x(\lambda_i)$ and $A_y(\lambda_j)$ directions by

$$A_x(\lambda_i^x) = \sqrt{\sum_j (F_{ij})^2} \tag{8}$$

and

$$A_y(\lambda_j^y) = \sqrt{\sum_i (F_{ij})^2} \ . \tag{9}$$

The amplitude spectra for maps at several frequencies are shown in Figures 10 and 11. These spectra allow comparison of the amplitude of the anomalies in the two

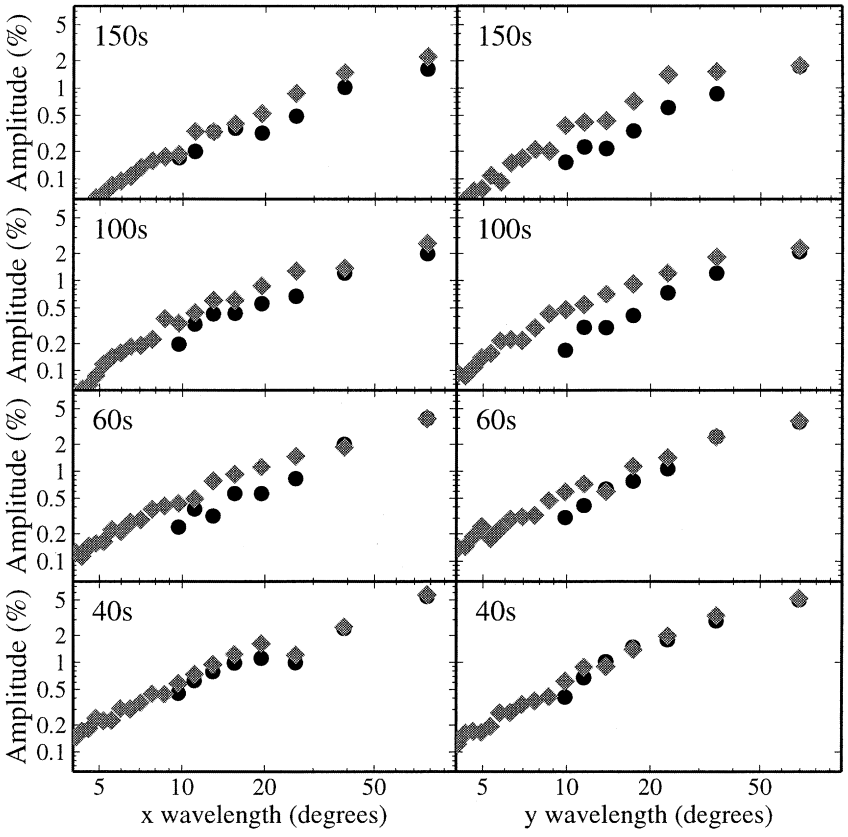

Figure 10
Spectra of Love-wave maps in Eurasia (computed in the large region in Fig. 9). Left panels are the amplitude spectra in the X direction (roughly east-west), and right panels are the amplitude spectra in the Y direction (roughly north-south). Circles are this study, diamonds are spectra of models from RITZWOLLER and LEVSHIN (1998). The period is in the upper left corner of each panel.

studies. We see excellent agreement between the two models, particularly for wavelengths longer than 30 degrees. At the shorter periods we see quite good agreement down to 15 degree wavelength. For shorter wavelengths, the global maps of this study consistently have lower amplitudes than the regional maps, especially for the long periods. The difference in amplitude for long-period Rayleigh waves is particularly large – the amplitude of the regional map is two to four times as large as the global map. To determine if this is due to our damping, we performed the inversions for Rayleigh waves without any damping. The effect on the amplitudes was insignificant for wavelengths longer than 1400 km. We return to discuss this discrepancy at the end of this section.

We calculate the correlation coefficient between the maps from the two studies at several different frequencies. The correlation coefficient, C, is defined in two dimensions by

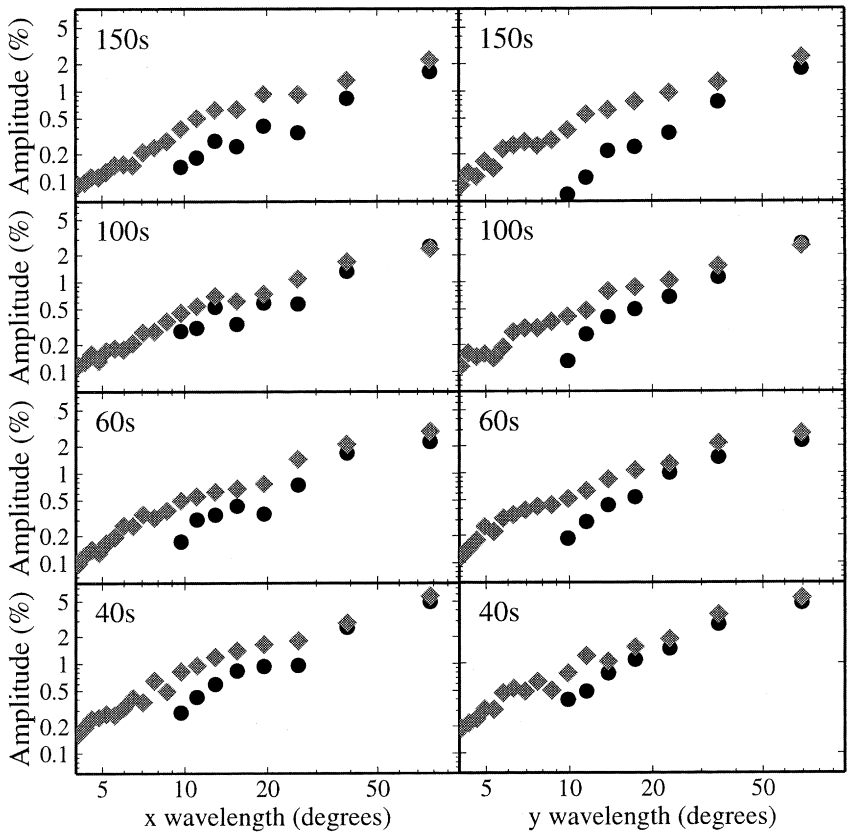

Figure 11
Spectra of Rayleigh-wave maps in Eurasia, see Figure 10 for an explanation.

$$C = \int_R \frac{f_1(\mathbf{r}) f_2(\mathbf{r})}{\sqrt{[f_1(\mathbf{r})]^2 + [f_2(\mathbf{r})]^2}} \, d^2\mathbf{r} \ , \tag{10}$$

where f_1 and f_2 are the functions we are comparing (after the average value of each has been removed) and R is the region of comparison. We first compare the models over the large region in Figure 9. As shown in Figures 12 and 13, the overall correlation coefficients are extremely high – between 0.8 and 0.9 for Rayleigh waves, and between 0.7 and 0.9 for Love waves. However, this correlation may be a function of agreement at long wavelengths. To investigate this, we have removed the long-wavelength structure from the maps to test the agreement at shorter length scales. We filtered the models to allow only features with wavelengths between 1000 and 3100 km (equivalent to degrees 13–40 of a spherical harmonic expansion). We determine the correlation between these filtered maps, and the correlation remains very good – well above the 99% confidence level. Even though most of the signal can be explained by only long-wavelength structure, the smaller features in the models still agree. The agreement between these models, which are derived from completely different data-sets, reinforces our conclusion from statistical tests that we are justified in modeling small-scale structure. We note that the Rayleigh-wave

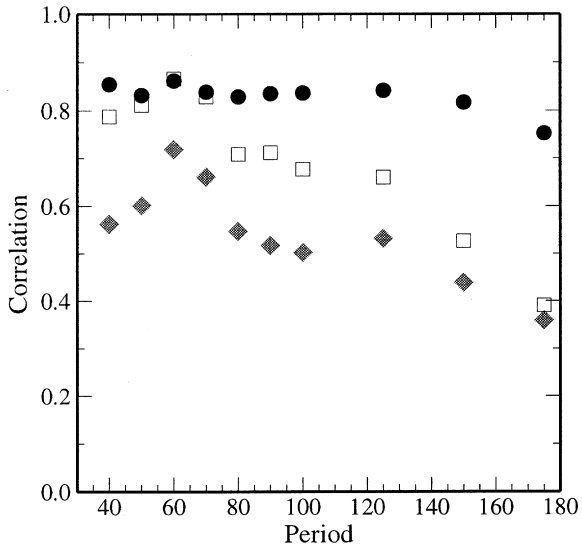

Figure 12
Correlation of Rayleigh-wave models in this study to models of RITZWOLLER and LEVSHIN (1998). Black circles are the total correlation in the large region of Figure 9, gray diamonds are the correlation for wavelengths 900–3000 km in the large region, and open squares are the correlation for wavelengths 900–3000 km in the small region. For the 145 parameters necessary to describe this resolution, the 99.99% confidence level is 0.32, and the 99% level is 0.25.

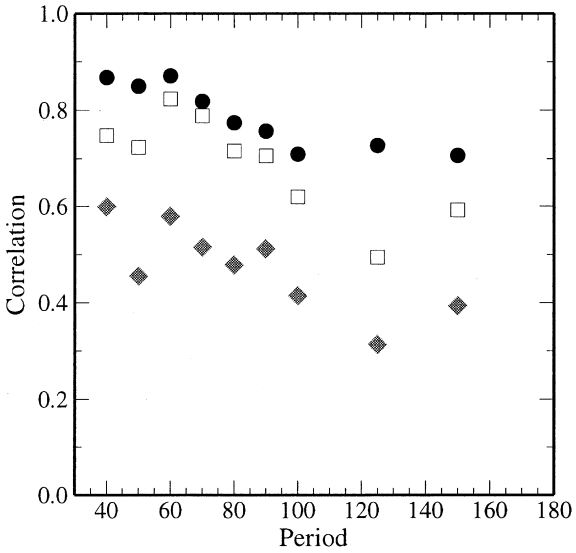

Figure 13
Correlation of Love-wave models in this study to models of RITZWOLLER and LEVSHIN (1998). See Figure 12 for explanation.

agreement is generally better, which is not surprising – Rayleigh-wave dispersion is easier to measure since these waves are recorded on the less-noisy vertical component. Also, because fundamental-mode Rayleigh waves have a low group velocity, they are easier to isolate from higher modes. However, the correlation plots show that the long-period models do not match as well, just as the comparison of spectra indicates.

Several possible reasons for the larger disagreement at long periods may be considered. As the period increases, surface waves become more sensitive to anomalies deeper in the earth, and typically the amplitude of the anomalies decreases with depth. Therefore, the signal is smaller, so the errors are relatively larger, which would lead to lower correlation between different models. However, the lower signal-to-error ratio is not sufficient to explain the large difference in amplitudes. There may be problems in the underlying dispersion-measurement technique for the long periods in either study. For long periods, it is more difficult to accurately measure the group velocity with short paths. Thus, the regional study may have larger errors at long periods and have insufficient damping to reduce the effect of errors. On the other hand, in this study, the smoothing constraints applied in the measurement of the phase-dispersion curve may limit the magnitude of the group velocity at long periods. Further research with different measurement methods will be necessary to determine the smaller-scale amplitudes at long periods.

6. Conclusions

We have produced global maps of surface-wave group velocity for both Love and Rayleigh waves in the period range 35 s to 175 s. The maps of group velocity can be useful for predicting the group arrival time of surface waves, which has applications in the location of earthquakes and explosions. These global models are particularly useful for monitoring purposes in regions where there are limited or no regional studies of group velocity, such as Africa and South America. The maps could also be used as starting models for regional studies to obtain even higher-resolution models where data coverage is sufficient.

At large scale-lengths, our new models agree well with previous work. In several regions, small features are shown which correlate well with variations that could be expected from surface geology. We have compared the maps to those of a regional study, and the correlation between the maps is extremely high. Global models are complementary to regional studies, as the quality of regional studies typically becomes poor near the edges of the model. Global models also provide information regarding less accessible regions of the Earth's surface.

Acknowledgements

We greatly appreciate the Generic Mapping Tools software (WESSEL and SMITH, 1998), which was used to produce all of the figures. This material is based upon work supported under a National Science Foundation Graduate Fellowship. We are grateful to M. Ritzwoller and A. Levshin for making digital versions of their maps easily available over the worldwide web. We thank J. Tromp and G. Laske for helpful discussions and for comments on this paper. We also extend appreciation to A. Curtis and A. Levshin for constructive reviews.

The degree 20 and degree 40 maps at all periods are available in several different formats from http://www.seismology.harvard.edu/projects/surfwave/LE00-Pageoph.

REFERENCES

CHEVROT, S., MONTAGNER, J. P., and SNIEDER, R. (1998), *The Spectrum of Tomographic Earth Models*, Geophys. J. Int. *133*(3), 783–788.

CURTIS, A., TRAMPERT, J., SNIEDER, R., and DOST, B. (1998), *Eurasian Fundamental Mode Surface Wave Phase Velocities and their Relationship with Tectonic Structures*, J. Geophys. Res. *103*(B11), 26,919–26,947.

DEMETS, C., GORDON, R. G., ARGUS, D. F., and STEIN, S. (1990), *Current Plate Motions*, Geophys. J. Int. *101*(2), 425–578.

DORMAN, J. *Seismic surface-wave data on the upper mantle*. In *The Earth's Crust and Upper Mantle*, Volume 13 of *Geophysical Monograph*, pp. 257–265 (Washington, DC, American Geophysical Union 1969).

DZIEWONSKI, A., CHOU, T., and WOODHOUSE, J. (1981), *Determination of Earthquake Source Parameters from Waveform Data for Studies of Global and Regional Seismicity*, Geophys. J. R. astr. Soc. *86*, 2825–2852.

DZIEWONSKI, A. M., and ANDERSON, D. L. (1981), *Preliminary Reference Earth Model*, Phys. Earth Planet. Int. *25*(4), 297–356.

DZIEWONSKI, A. M., BLOCH, S., and LANDISMAN, M. (1969), *A Technique for the Analysis of Transient Seismic Signals*, Bull. Seismol. Soc. Am. *59*(1), 427–444.

EKSTRÖM, G., TROMP, J., and LARSON, E. W. F. (1997), *Measurements and Global Models of Surface Wave Propagation*, J. Geophys. Res. *102*(B4), 8137–8157.

KEILIS-BOROK, V. I. (ed.) *Seismic Surface Waves in a Laterally Inhomogeneous Earth*. (Norwell, mass: Kluwer Academic Publishers 1989).

KNOPOFF, L., and SCHWAB, F. A. (1968), *Apparent Initial Phase of a Source of Rayleigh Waves*, J. Geophys. Res. *73*, 755–760.

LARSON, E. W. F., TROMP, J., and EKSTRÖM, G. (1998), *Effects of Slight Anisotropy on Surface-wave Propagation*, Geophys. J. Int. *132*(3), 654–666.

LASKE, G., and MASTERS, G. (1996), *Constraints on Global Phase Velocity Maps from Long-period Polarization Data*, J. Geophys. Res. *101*(B7), 16,059–16,075.

LEVSHIN, A., RATNIKOVA, L., and BERGER, J. (1992), *Peculiarities of Surface-wave Propagation across Central Eurasia*, Bull. Seismol. Soc. Am. *82*(6), 2464–2493.

LEVSHIN, A. L., RITZWOLLER, M. H., and RESOVSKY, J. S. (1999), *Source Effects on Surface Wave Group Travel Times and Group Velocity Maps*, Phys. Earth Planet. Int. *115*(3–4), 293–312.

LEVSHIN, A. L., YANOVSKAYA, T. B., LANDER, A. V., BUKCHIN, B. G., BARMIN, M. P., RATNIKOVA, L. I., and ITS, E. N. (1989), *Seismic Surface Waves in a Laterally Inhomogeneous Earth*, Chapter 5. In Keilis-Borok (1989).

MONTAGNER, J.-P., and TANIMOTO, T. (1990), *Global Anisotropy in the Upper Mantle Inferred from the Regionalization of Phase Velocities*, J. Geophys. Res. *95*, 4797–4819.

MUYZERT, E., and SNIEDER, R. (1996), *The Influence of Errors in Source Parameters on Phase Velocity Measurements of Surface Waves*, Bull. Seismol. Soc. Am. *86*(6), 1863–1872.

NISHIMURA, C. E., and FORSYTH, D. W. (1988), *Rayleigh Wave Phase Velocities in the Pacific with Implications for Azimuthal Anisotropy and Lateral Heterogeneities*, Geophys. J. R. astr. Soc. *94*, 479–501.

PASSIER, M. L., and SNIEDER, R. K. (1995), *On the Presence of Intermediate-scale Heterogeneity in the Mantle*, Geophys. J. Int. *123*(3), 817–837.

PRESS, W. H., TEUKOLSKY, S. A., VETTERLING, W. T., and FLANNERY, B. P., *Numerical Recipies in C: The Art of Scientific Computing* (2nd edn.) (Cambridge University Press 1992).

RITZWOLLER, M. H., and LEVSHIN, A. L. (1998), *Eurasian Surface Wave Tomography: Group Velocities*, J. Geophys. Res. *103*(B3), 4839–4878.

ROSA, J. W. C., (1987), *A Global Study on Phase Velocity, Group Velocity and Attenuation of Rayleigh Waves in the Period Range 20 to 100 Seconds*, Ph. D. Thesis, Massachusetts Institute of Technology, Cambridge, MA, USA.

TRAMPERT, J., and WOODHOUSE, J. H. (1995), *Global Phase Velocity Maps of Love and Rayleigh waves between 40 and 150 Seconds*, Geophys. J. Int. *122*, 675–690.

TRAMPERT, J., and WOODHOUSE, J. H. (1996), *High Resolution Global Phase Velocity Distributions*, Geophys. Res. Lett. *23*(1), 21–24.

VAN HEIJST, H. J., and WOODHOUSE, J. H. (1999), *Global High Resolution Phase Velocity Distributiuons of Overtone and Fundamental Mode Surface Waves Determined by Mode Branch Stripping*, Geophys. J. Int. *137*, 601–620.

WANG, Z., and DAHLEN, F. (1995), *Validity of Surface-Wave Ray Theory on a Laterally Heterogeneous Earth*, Geophys. J. Int. *123*, 757–773.

WANG, Z., TROMP, J., and EKSTRÖM, G. (1998), *Global and Regional Surface-wave Inversions; A Spherical-spline Parameterization*, Geophys. Res. Lett. *25*(2), 207–210.

WESSEL, P., and SMITH, W. H. F. (1998), *New, Improved Version of the Generic Mapping Tools Released*, EOS Trans. AGU *79*(47), 579.

ZHANG, Y.-S., and LAY, T. (1996), *Global Surface Wave Phase Velocity Variations*, J. Geophys. Res. *101*(B4), 8415–8436.

(Received June 30, 1999, revised February 5, 2000, accepted March 1, 2000)